Energy & Environmental Science

Accepted Manuscript

This article can be cited before page numbers have been issued, to do this please use: D. Zhao, X. Yu, J. Wang, Q. Gao, Z. Wang, T. Cheng and Z. L. Wang, *Energy Environ. Sci.*, 2022, DOI: 10.1039/D2EE01553F.

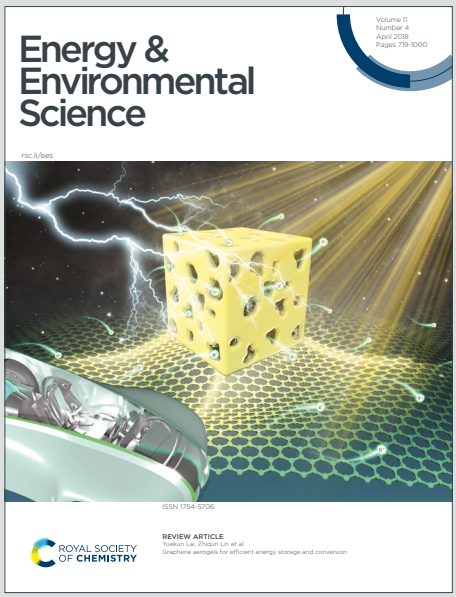

ROYAL SOCIETY OF CHEMISTRY

rsc.li/ees

View Article Online
DOI: 10.1039/D2EE01553F

Broader context

Triboelectric nanogenerators (TENGs) are a core technology in micro/nano power sources and self-powered sensing, as well as blue energy and high-voltage sources. And the output performance of TENGs is affected by their mechanical structures (*e.g.* contact area, film thickness) and external excitations (*e.g.* applied force, displacement distance, triggering frequency). However, the importance of influencing factors on output performance has not been well investigated. Moreover, the influence mechanism of various factors has not been clearly explained. Therefore, a standard for normalizing the outputs of triboelectric nanogenerators in various modes is proposed in this paper. The internal components of the equivalent circuit model are shown more clearly, and the normalization method based on the equivalent circuit model is used for the first time to clarify the influence rules and working mechanism of these factors on TENG outputs. This research will be meaningful to identify appropriate factors, achieve higher output performance and improve energy conversion efficiency for TENGs in various modes.

View Article Online
DOI: 10.1039/D2EE01553F

ARTICLE

A standard for normalizing the outputs of triboelectric nanogenerators in various modes

Received 00th January 20xx,
Accepted 00th January 20xx

DOI: 10.1039/x0xx00000x

Da Zhao,‡[ab] Xin Yu,‡[a] Jianlong Wang,‡[ab] Qi Gao,[a] Zhenjie Wang,[a] Tinghai Cheng *[ab] and Zhong Lin Wang *[ac]

A quantitative standard based on the internal equivalent circuit is proposed to evaluate the effects of different factors on the outputs of the triboelectric nanogenerators (TENGs) in various modes. This paper establishes the relationship between the equivalent circuit and TENGs, and then explores the influence of mechanical structures (*e.g.* contact area, film thickness) and external excitations (*e.g.* applied force, displacement distance, triggering frequency) on output power and matching reactance by the normalization method. Moreover, the prototypes are fabricated to verify the rationality and feasibility of normalization. Experimental results show that the importance of influencing factors is: contact area > film thickness > applied force > displacement distance. The influence of frequency on the normal-directional moving TENG is greater than that of tangential-directional moving TENG. This work provides a reference for quantifying the outputs of TENGs with different structures.

Broader context

Triboelectric nanogenerators (TENGs) are a core technology in micro/nano power sources and self-powered sensing, as well as blue energy and high-voltage sources. And the output performance of TENGs is affected by their mechanical structures (*e.g.* contact area, film thickness) and external excitations (*e.g.* applied force, displacement distance, triggering frequency). However, the importance of influencing factors on output performance has not been well investigated. Moreover, the influence mechanism of various factors has not been clearly explained. Therefore, a standard for normalizing the outputs of triboelectric nanogenerators in various modes is proposed in this paper. The internal components of the equivalent circuit model are shown more clearly, and the normalization method based on the equivalent circuit model is used for the first time to clarify the influence rules and working mechanism of these factors on TENG outputs. This research will be meaningful to identify appropriate factors, achieve higher output performance and improve energy conversion efficiency for TENGs in various modes.

Introduction

In recent years, researchers have shown an increased interest in energy harvesting and supply by using triboelectric nanogenerators (TENGs),[1,2] which are becoming the core technology in related fields.[3,4] However, the output performance of TENGs is limited by various factors such as contact area, film thickness, displacement distance, applied force and triggering frequency. In addition, the working mode of TENGs also was an important factor in affecting the output performance,[5,6] which is divided into four types: the contact-separation (C-S), single-electrode (S-E), lateral-sliding (L-S) and free-standing (F-S) mode, respectively.[7-10] Therefore, researching on various factors is a key issue in improving the output performance of TENGs[11,12] and expanding their applications.[13-15]

[a] *Beijing Institute of Nanoenergy and Nanosystems, Chinese Academy of Sciences, Beijing 101400, P. R. China. E-mail: chengtinghai@binn.cas.cn.*
[b] *School of Mechatronic Engineering, Changchun University of Technology, Changchun, Jilin 130012, P. R. China.*
[c] *School of Materials Science and Engineering, Georgia Institute of Technology, Atlanta, GA 30332-0245, USA. E-mail: zhong.wang@mse.gatech.edu.*
† Electronic Supplementary Information (ESI) available. See DOI: 10.1039/x0xx00000x
‡ These authors contributed equally to this work.

View Article Online
DOI: 10.1039/D2EE01553F

The mechanical structures (*e.g.* contact area, film thickness) and external excitations (*e.g.* displacement distance, applied force and triggering frequency) of TENGs have been thought as the important factors in affecting the output power.[16-20] Extensive researches have shown an increasing interest in the influence of various factors on output performance.[21,22] And the change of mechanical structures affects the total surface charges to change the output performance of TENGs.[23,24] Moreover, it has been reported that the peak power of TENGs increases with the increase of external excitations such as the displacement distance, applied force and triggering frequency.[25] These investigations confirmed that the above factors can affect the internal resistance and output performance of TENGs.[26-28] There are a few research literatures that reveal the importance of various factors for TENG outputs. However, recent evidence displays that the material selection of direct current TENG is solved by a normalization method,[29] so that the outputs of different TENGs can be evaluated and compared. Moreover, many researchers have widely utilized normalization to evaluate performance in mathematics and engineering. Hence, it is necessary to propose a normalization method to judge the influence of various factors on the output performance.

In order to explore the influence degree of mechanical structures and external excitations on the output performance, a quantitative standard is proposed based on equivalent circuit model. This paper analyses the relationship between the equivalent circuit and the structure of TENG in various modes, and establishes the theory of the normalization method. Moreover, the experiments explore the influence of mechanical structures (*e.g.* contact area, film thickness) and external excitations (*e.g.* applied force, displacement distance, triggering frequency) on output power and matching reactance by the normalization method. In addition, four prototypes with different working modes are used to verify the feasibility of the normalization method by combining theory and experiment.

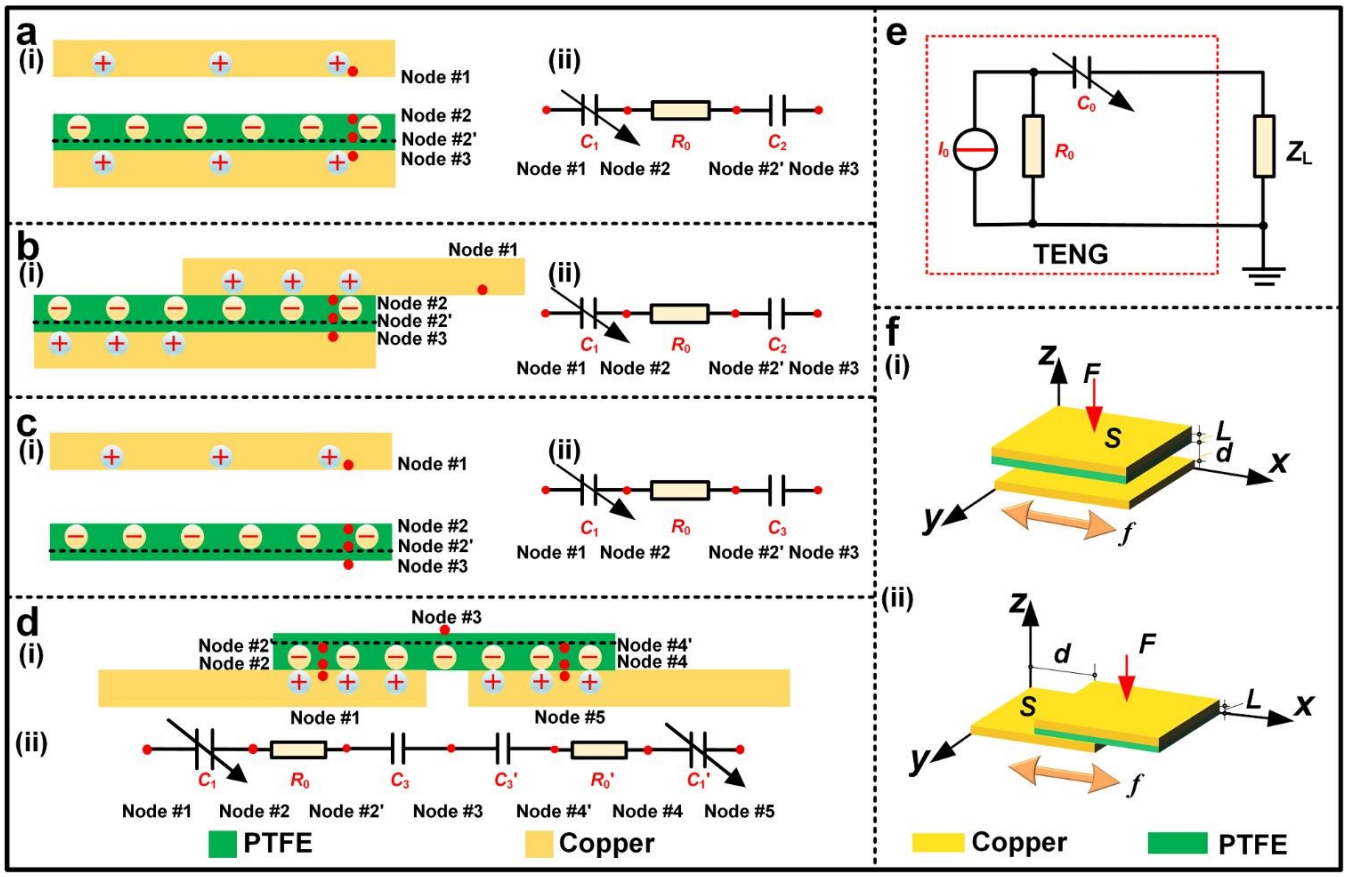

Fig. 1. Schematic structures and the equivalent circuit model for TENGs in the (**a**) contact-separation mode (C-S mode), (**b**) lateral-sliding mode (L-S mode), (**c**) single-electrode mode (S-E mode), (**d**) free-standing mode (F-S mode), (**e**) equivalent circuit model, and (**f**) parameters of C-S mode (**i**) and L-S mode (**ii**).

View Article Online
DOI: 10.1039/D2EE01553F

Theoretical analysis

Structure of internal equivalent circuit.

The analysis of the equivalent circuit model plays a key role in the normalization of various factors. It is necessary to study the relationship between the equivalent circuit and the structure of TENGs. The effect of capacitance and resistance is analyzed by the node method, as shown in Fig. 1 and Fig. S1 (ESI†). For C-S mode TENG, the variable capacitance C_1, triboelectric layer[30] and constant capacitance C_2 are constituted between nodes #1 and #2, #2 and # 2' as well as # 2 and #3, respectively (Fig. 1a). Moreover, due to the interaction of triboelectric charges, internal resistance R_0 is formed in the triboelectric layer. Due to the presence of the triboelectric layer, an internal resistance of single molecular thickness is formed. Furthermore, the triboelectric layer plays a crucial role in maintaining triboelectric charge, as well as providing power, as it forms the induction charge, variable capacitance, and constant capacitance. Therefore, the equivalent circuit consists of C_1, R_0 and C_2. Similarly, the internal circuit of L-S mode TENG is the same as C-S mode TENG (Fig. 1b). For S-E mode TENG, the inductive capacitance C_3 between the dielectric layer and the substrate replaces the constant capacitance C_2 in Fig. 1c. For F-S mode, Node #1, #2 and Node #4, #5, respectively form two variable capacitances C_1 and C_1' with opposite changes. And Node #2, #2' and Node #4, #4' constitute two triboelectric layers, whereby the resistances R_0 and R_0' are formed on the surface of the dielectric layer.[31] Furthermore, two inductive capacitances C_3 and C_3' are composed between Node #2', #3 and Node #3, #4' (Fig. 1d).

In addition, the triboelectric layer is generally composed of molecular layers. Therefore, the internal resistance length T is the thickness of the monolayer according to the resistance equation $R=\rho T/S$. The circuit is simplified and power supply is added to generate the equivalent circuit model of TENGs in Fig. 1e. The output performance and internal circuit of TENG are affected by mechanical structures such as contact area S and film thickness L, and external excitations such as displacement distance d, applied force F and triggering frequency f (Fig. 1f). The relationship between various factors and each internal component in the equivalent circuit model is established. By combining circuit theory and an equivalent circuit model, the normalization theory can be formed.

Normalization theory

According to the equivalent circuit model of TENGs, the load current I^1 of matching resistance R^L and matching capacitor C^L is derived:

$$V_R = I_1\sqrt{R_L^2+\left(\frac{1}{2\pi f}\left(\frac{1}{C_1}+\frac{1}{C_2}\right)\right)^2} \quad (1)$$

$$V_C = I_1\frac{1}{2\pi f}\left(\frac{1}{C_1}+\frac{1}{C_2}+\frac{1}{C_L}\right) \quad (2)$$

where R^L, C^0, C^L stand for internal current, load resistance, internal capacitance, and load capacitance, respectively. V_R, V_C are the total voltage of TENG under load resistance and capacitance. Moreover, the definitions of the key parameters of the TENG are presented in Table S1 (ESI†).

The power of the load resistance P^R (Eqs. S1, 3) (ESI†) and capacitance P^C (Eqs. S2, 4) (ESI†) can be obtained by equations $P^R = I_1^2 R_L$ and $P^R = I_1 U_C$, and resistance and capacitance equation $R = \rho T/S$ and $C^0 = \varepsilon^r S/4\pi kd$. It is deduced that:

$$P_R = \frac{\left(\frac{\sigma S}{t}\right)^2\left(\rho\frac{T}{S}\right)^2 R_L}{R_L^2+\left(\frac{1}{2\pi f}\left(\frac{4\pi kL}{\varepsilon_{r1}S}+\frac{4\pi kD}{\varepsilon_{r2}S}\right)\right)^2} \quad (3)$$

$$P_C = \frac{\left(\frac{\sigma S}{t}\right)^2\left(\rho\frac{T}{S}\right)^2\left(\frac{1}{2\pi f C_L}\right)}{\left(\frac{1}{2\pi f}\left(\frac{4\pi kL}{\varepsilon_{r1}S}+\frac{4\pi kD}{\varepsilon_{r2}S}+\frac{1}{C_L}\right)\right)^2} \quad (4)$$

where σ, t, ρ, T, k, ε^{r1} and ε^{r2} mean charge density, time of current changes, the resistivity of the dielectric layer, the film thickness, the electrostatic force constant, the relative dielectric constant of the dielectric layer and the environment, respectively. The variable capacitance is the largest when the displacement distance is the smallest, so D is the minimum displacement distance and the peak power of TENG is the largest.

It can be obtained that the reactance matching value a^g of the internal reactance and the external reactance.

$$Z_i = \sqrt{(R_0)^2+\left(\frac{1}{j\omega}\left(\frac{1}{C_1}+\frac{1}{C_2}\right)\right)^2} \quad (5)$$

$$a_g = \frac{R_L}{Z_i} = \frac{R_L}{\sqrt{(R_0)^2+\left(\frac{1}{j\omega}\left(\frac{1}{C_1}+\frac{1}{C_2}\right)\right)^2}} \quad (6)$$

Ignoring the edge effect, Eq. (7) is derived by using the equation of resistance and capacitance:

$$\begin{cases} a_g = \dfrac{R_L}{\sqrt{\left(\rho\cdot\dfrac{T}{S}\right)^2+\left(\dfrac{2k}{fS}\left(\dfrac{L}{\varepsilon_{r1}}+\dfrac{D}{\varepsilon_{r2}}\right)\right)^2}} \\ a_g = \dfrac{\left(\dfrac{1}{2\pi f C_L}\right)}{\sqrt{\left(\rho\dfrac{T}{S}\right)^2+\left(\dfrac{2k}{fS}\left(\dfrac{L}{\varepsilon_{r1}}+\dfrac{D}{\varepsilon_{r2}}\right)\right)^2}} \end{cases} \quad (7)$$

The influence matching value of each factor is shown in Supplementary Note 1.

Combining Eqs. (S3, S4) (ESI†), Eq. (8) is expressed for contact area *S*.

$$\begin{cases} \Delta R_L = \alpha_s \cdot \dfrac{1}{\Delta S} \\ \Delta C_L = \dfrac{1}{2\pi f}\cdot\dfrac{1}{\alpha_s}\cdot\Delta S \end{cases} \quad (8)$$

The internal resistance of TENGs is about MΩ level. Due to its much lower reactance than constant capacitance, internal resistance is numerically negligible. Moreover, the two output peaks of TENGs occur in the contact and the maximum separation states, respectively. And one of the single-direction pulses is affected by the change in film thickness.[19,32] The variable capacitance remains unchanged when the displacement distance is constant. When the two electrodes are in contact, the pulse affected by the thickness of the film appears as a peak for normal-directional moving TENGs, so the relative distance of the variable capacitance is less than the film thickness.[33,34] For tangential-directional moving TENGs, because the electrodes remain in contact and the variable capacitance is less than the constant capacitance, the variable capacitance can also be ignored numerically.

According to above reasons and Eqs. (S5, S6) (ESI†), Eq. (9) can be obtained for the film thickness *L*.

$$\begin{cases} \Delta R_L \approx \beta_L \cdot \Delta L \\ \Delta C_L \approx \dfrac{1}{2\pi f \beta_L}\cdot\dfrac{1}{\Delta L} \end{cases} \quad (9)$$

At the maximum displacement, other single-direction peak pulse of normal-directional moving TENGs occurs. And as the spacing of the constant capacitance is less than that of the variable capacitance, it can be ignored. However, the displacement distance of tangential-directional moving TENGs is related to contact area, so $S = ad$. a is the side length. Eq. (10) is derived by Eqs. (S7-S9) (ESI†).

$$\begin{cases} \Delta R_L \approx \theta_{d1}\Delta d & \text{(C-S \& S-E modes)} \\ \Delta R_L \approx \dfrac{\theta_{d1}}{\Delta d} & \text{(L-S \& F-S modes)} \\ \Delta C_L \approx \dfrac{1}{2\pi f}\cdot\dfrac{1}{\theta_{d2}}\cdot\dfrac{1}{\Delta d} & \text{(C-S \& S-E modes)} \\ \Delta C_L \approx \dfrac{1}{2\pi f}\cdot\dfrac{1}{\theta_{d2}}\cdot\Delta d & \text{(L-S \& F-S modes)} \end{cases} \quad (10)$$

In the case of ignoring internal resistance and variable capacitance, Eq. (11) is expressed according to Eqs. (S10-S11) (ESI†) for applied force *F*. That the applied force is proportional to the contact area and inversely proportional to the film thickness can be explained according to stress formula $\delta = F/S$ and compression deformation equation $\Delta L = FL/ES$. E is elastic modulus.

$$\begin{cases} \Delta R_L \approx \lambda_F \cdot \Delta\left(\dfrac{L}{S}\right) \\ \Delta C_L \approx \dfrac{1}{2\pi f}\cdot\dfrac{1}{\lambda_F}\cdot\Delta\left(\dfrac{S}{L}\right) \end{cases} \quad (11)$$

For triggering frequency *f*, normalization of reactance is expressed in Eq. (12) combining with Eqs. (S12, S13) (ESI†).

$$\begin{cases} \Delta R_L \approx \dfrac{\omega_f}{\Delta f} \\ \Delta C_L \approx \dfrac{1}{2\pi}\cdot\dfrac{1}{\omega_f} \end{cases} \quad (12)$$

The normalization modes of load voltage and current are shown in Eqs. (S14, S15) (ESI†).

By combining with the above formula, the load resistance and load capacitance in the experiment are proportionally transformed. Therefore, the optimal matching resistance and matching capacitance are normalized to the identical value.

Generally speaking, the contact area is relevant to all equivalent circuit devices in TENG. And the film thickness and displacement distance are only related to the constant capacitance and variable capacitance, respectively. Moreover, triggering frequency and applied force affect constant and variable capacitance.

Results and discussion

Normalization of matching reactance for the mechanical structures

The mechanical structures of TENGs include contact area and film thickness. In Fig. 2a, b, the peak power increases rapidly as the contact area increases, and the

View Article Online
DOI: 10.1039/D2EE01553E

match resistance declines while the match capacitance increases. The film thickness of TENG is inversely proportional to the peak power, the matching resistance increases and the capacitance decreases in Fig. 2c, d. The charge transfer mechanism is presented in Fig. 2e as the contact area and film thickness increase.

Supplementary Fig. 2 shows that the surface charges increase at the dielectric layer as the contact area increases, as well as the load voltage and current. According to Eq. (8), the matching resistance is inversely proportional to the contact area. Similarly, the larger the contact area, the greater the internal matching capacitance (Fig. S2a, b) (ESI†). As the film thickness increases, the induced charges are reduced, and the load voltage and current decrease in Supplementary Fig. 2c, d. It follows from Eq. (9), that the film thickness is proportional to the matching resistance, while the matching capacitance decreases as the film thickness increases. The change regulations of output performance for S-E and F-S mode are consistent with that for C-S and L-S mode under different mechanical structures (Figs. S3 and S4) (ESI†).

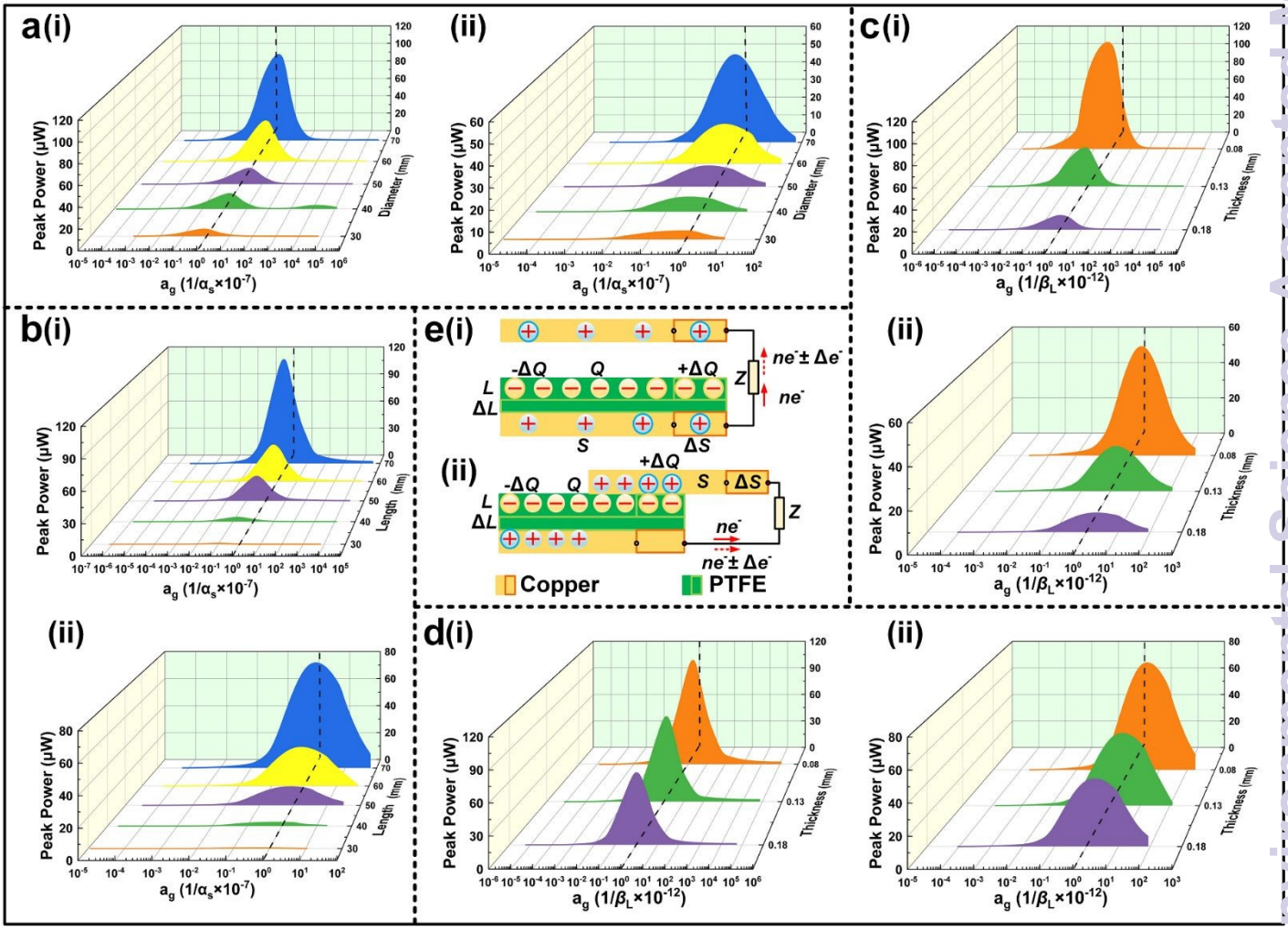

Fig. 2. Normalized analysis of output performance under different resistances (**i**) and capacitances (**ii**) for contact area (**a, b**) and film thickness (**c, d**) in C-S (**a, c**) and L-S (**b, d**) mode TENGs. (**e**) Diagram of charge transfer in C-S and L-S mode TENGs with changes in contact area and film thickness.

Normalization of matching reactance for the external excitations

Among the external excitations of TENGs are the displacement distance, the applied force and the triggering frequency. The Fig. 3a, b presents the results of normalizing the outputs for the C-S and L-S modes under different displacement distances. For displacement distance, the normal-directional moving mode (C-S and S-E mode) is different from tangential moving mode (L-S and F-S mode). It is the plate distance of a variable capacitance which determines the

View Article Online
DOI: 10.1039/D2EE01553F

displacement distance for the normal moving mode. Triboelectric contact area and output performance gradually increase as the displacement distance for tangential moving mode increases. In addition, the output performance and the transferred charges increase as the displacement distance increases.

On the other hand, according to Hooke's law ($\delta = F/S$) and the deformation law ($\Delta L = FL/ES$), an increase in applied force would result in an expansion of the real contact area and a reduction in film thickness. Therefore, it can be seen from Fig. S3c, d (ESI†) that with the elevation of applied force, the outputs gradually rise, the matching resistance lowers, and the matching capacitance grows. Charge transfer is illustrated in Fig. 3e under different displacement distances and applied forces. The load voltage and current are displayed in Supplementary Figs. 5 and 6 as displacement distance and force change. Moreover, normalizing outputs are shown in Supplementary Fig. 7 under displacement distance and applied force for S-E and F-S mode TENGs.

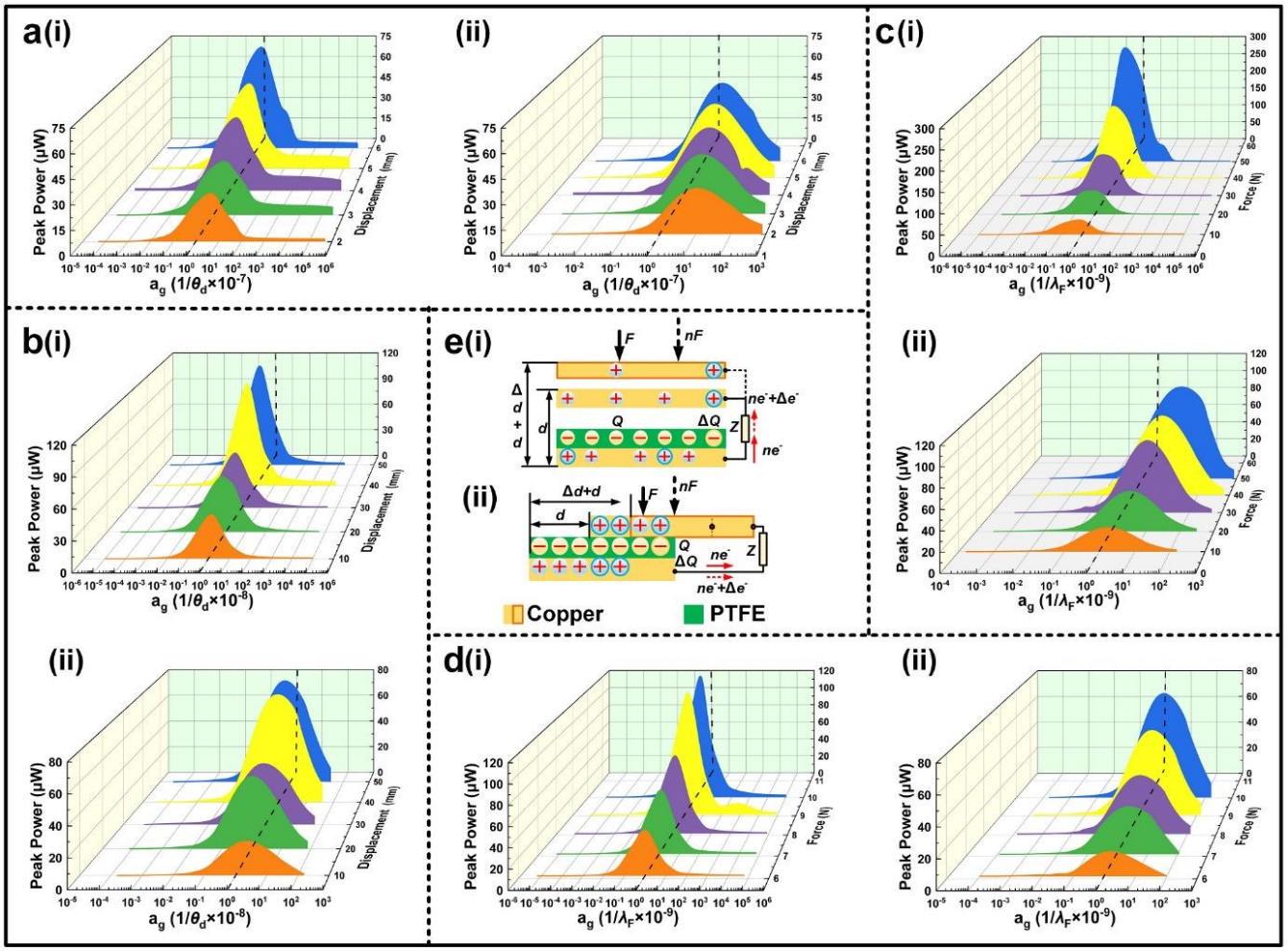

Fig. 3. Normalizing outputs under different resistances (**i**) and capacitances (**ii**) for displacement distance (**a, b**) and applied force (**c, d**) in C-S (**a, c**) and L-S (**b, d**) mode TENGs. (**e**) Schematic diagram of C-S and L-S mode changing with displacement distance and applied force.

Fig. 4a depicts the charge transfer mechanism with a change in triggering frequency for the C-S and L-S modes TENGs. In Fig. 4b, c and Supplementary Fig. S8, the outputs of C-S and L-S mode TENGs are normalized with triggering frequency according to Eq. (13). The results of the research indicate that the matching capacitance remains constant with changes in frequency. Furthermore, the matching resistance declines as the triggering frequency increases. The outputs and normalized data of S-E and F-S mode TENGs are shown in Figs. S9 and S10 (ESI†), and these are similar to C-S and L-S mode TENGs.

As shown in Fig. 4d, e and Fig. S10d, e (ESI†) the trends of different load voltages and currents with triggering frequency can be seen. In experimental tests, the trigger frequency varied between 15 and 180 r/min

by uniform acceleration or deceleration. In the case of external resistance less than GΩ, the load voltage is proportional to the triggering frequency. Differently, when the resistance is greater than GΩ, the load voltage remains constant as the triggering frequency increases. At low resistance, the charges can pass through the external load resistance normally, which means the voltage rises as the current grows. The internal resistance of TENGs is generally at MΩ level. When the load resistance significantly exceeds the internal resistance, the load current approaches zero. Furthermore, the surface charges of TENGs would be directly driven into the test equipment, which is a capacitive device. Consequently, the voltage does not change with frequency when the resistance exceeds the MΩ level.[10,35,36] By Ohm's law, the load voltage is unrelated to frequency, so it remains unchanged for load capacitance. Moreover, the load current increases with an improvement in triggering frequency. According to the definition of current, it represents an increase in the rate of charge transfer, so the current is directly proportional to the frequency. All in all, as the trigger frequency increases, surface charges transfer more quickly, but the total transferred charge remains invariable. Therefore, the time of charge transfer is the key to improving outputs for triggering frequency.

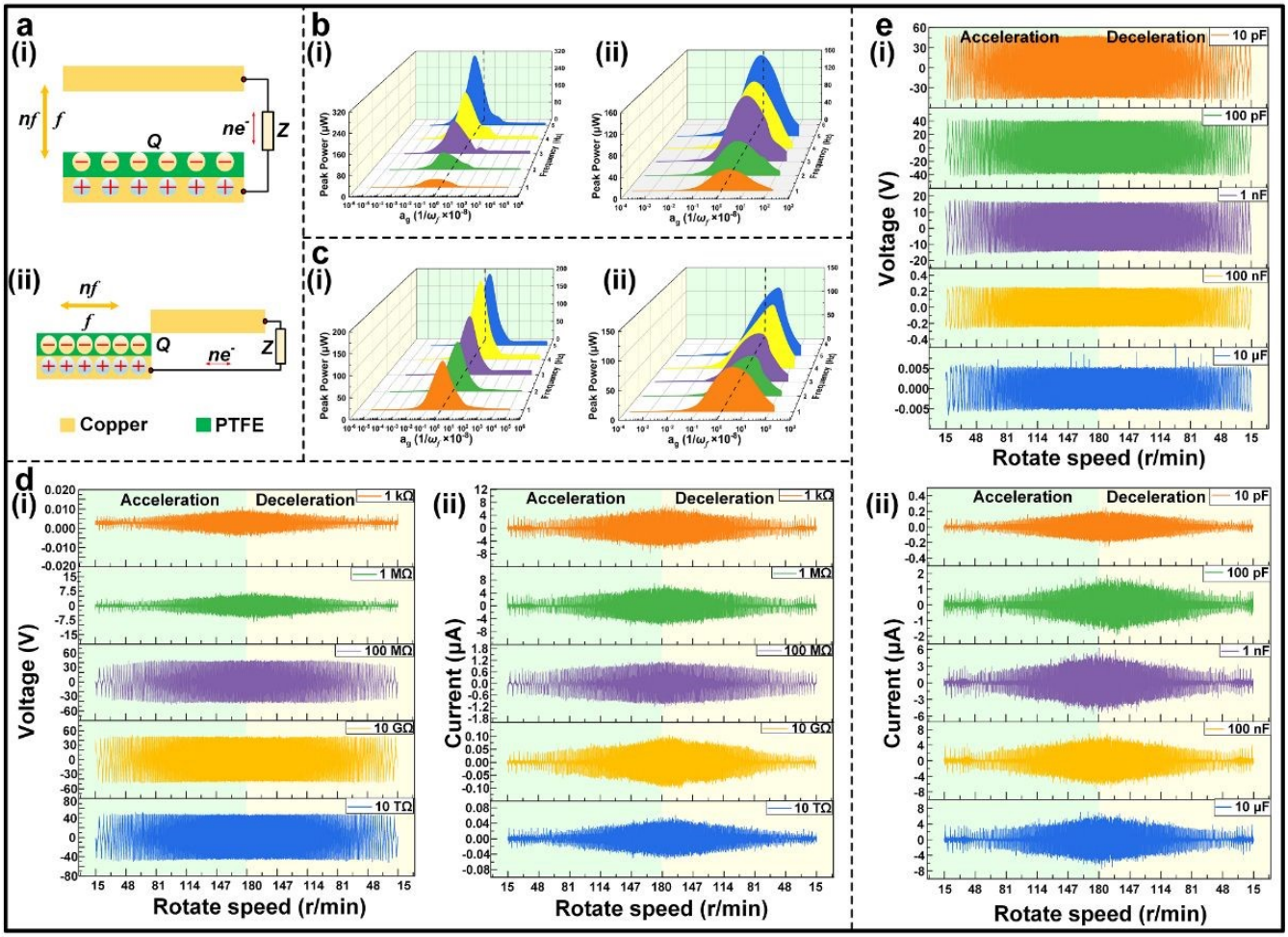

Fig. 4. Normalizing outputs under different resistances (**i**) and capacitances (**ii**) for triggering frequency in C-S (**b**) and L-S (**c**) mode TENGs. (**a**) Schematic diagram of C-S (**i**) and L-S (**ii**) mode TENGs changing with triggering frequency. (**d, e**) The output performance of TENGs as triggering frequency changes under different resistances (**d**) and capacitances (**e**).

Normalization of the output power for TENGs

As shown in Fig. 5, Fig. S11 and Table S2 (ESI†), the output power is normalized under various factors such as contact area, film thickness, displacement distance, applied force and triggering frequency. The results indicate that the order of importance is: contact area > film thickness > application force > displacement distance. In relation to the four modes TENGs, contact area is the most significant factor, and power is

View Article Online
DOI: 10.1039/D2EE01535E

proportional to contact area. The degree of influence of the contact area on performance is approximately 99.56%. The charges grow as the contact area increases, which is the determining factor for power output. Moreover, the film thickness has the impact on the amount of induced charges for the TENGs. As a result of the working principle of TENGs, the outputs are inversely proportional to the induced charges. Furthermore, the output power depends on the transferred charge under different displacement distances. As the transferred charge is limited, the output power grows slowly as the displacement distance rises. And tangential moving modes have a significantly higher influence degree than normal-directional moving modes. The main reason is that the displacement of the tangential and normal-directional moving modes changes the contact area and the distance of the variable capacitance, respectively. Also, as the displacement distance grows, the induced charge declines for the L-S mode and both electrodes in F-S mode generate more triboelectric charges. The displacement distance has a lesser impact on the L-S mode than the F-S mode. According to Hooke's law and the deformation law, the increase in applied force would increase the contact area and reduce the film thickness. Therefore, triboelectric and induced charges are accumulated and the outputs are also enhanced with increasing applied force. Overall, according to the above key factors, the output performance can be adjusted by changing the amount of triboelectric and induced chargers in the system. Moreover, mechanical structures have a more significant influence on performance than external excitations. For external excitations, the outputs are changed by altering mechanical structures. Therefore, the order of influencing factors is as follow: contact area > film thickness > applied force > displacement distance.

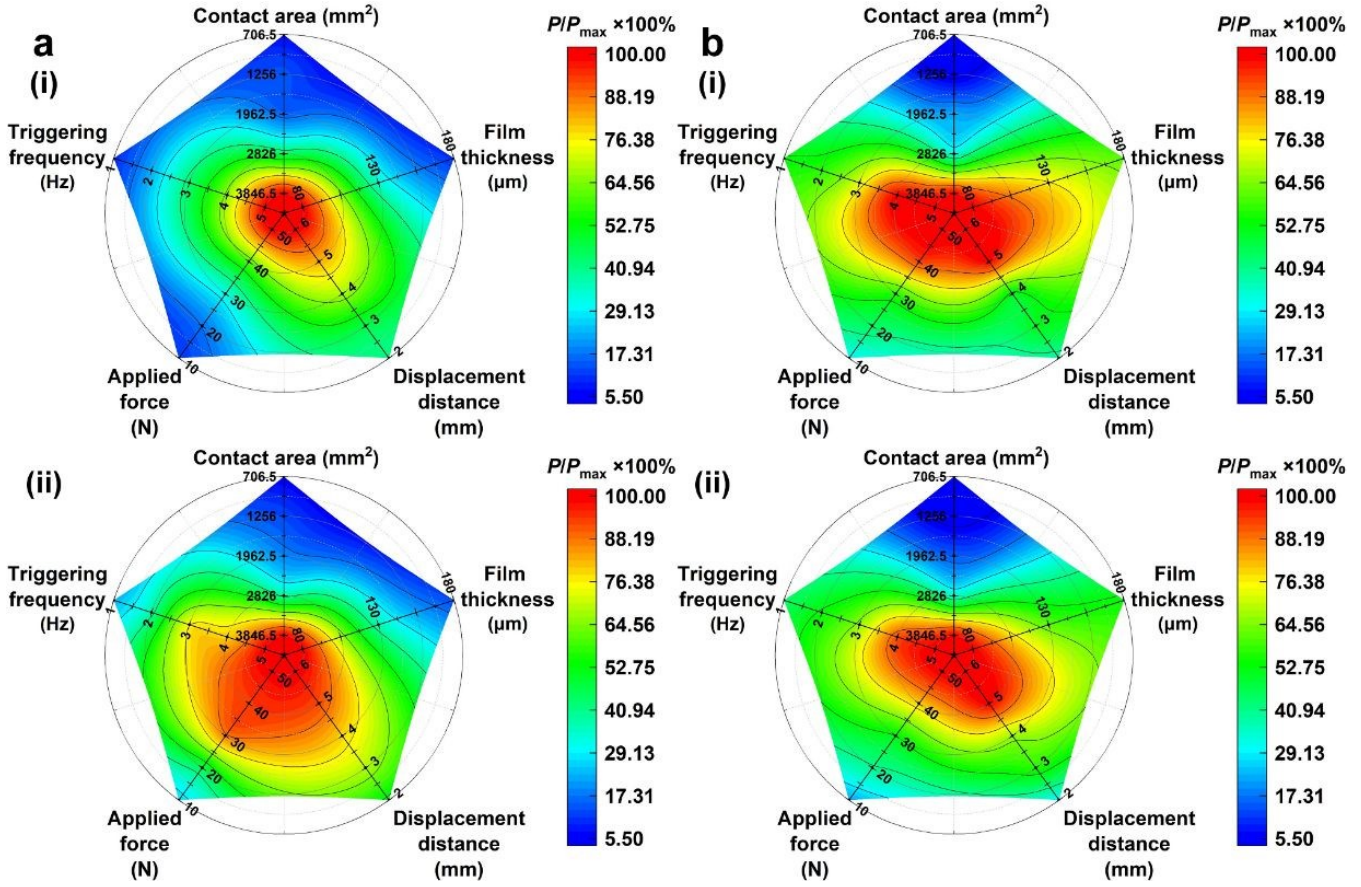

Fig. 5. Normalization of optimal peak power for TENGs of C-S mode (**a**) and L-S mode (**b**) under different load resistance (**i**) and capacitance (**ii**).

On the other hand, the outputs of TENGs are mainly improved when the triggering frequency increases by reducing the time of charge moving direction and increasing the change speed of variable capacitance.

View Article Online
DOI: 10.1039/D2EE01553E

Additionally, the normal-directional moving TENGs is more influenced by triggering frequency than tangential-directional moving TENGs. For normal-directional moving TENGs, the charges change instantaneously as the touch between the electrodes is instantaneous in the triboelectric layer. Moreover, because the triboelectric layer is linear and slow to touch, the triboelectric charges of tangential-directional moving TENGs would gradually transfer. Therefore, the influence degree of normal-directional moving TENGs changes more significantly with the triggering frequency. In addition, the output voltage and current of the load resistance are affected by the triggering frequency to some extent. However, triggering frequency only impacts load current of capacitance. As a result, the load capacitance is less subject to changes in triggering frequency than the load resistance.

Tangential-directional moving TENGs rely more on the contact area and its related external excitations than normal-directional moving TENGs. In contrast, film thickness and its related external excitations are different from the contact area. Due to the high triboelectric charge of tangential-directional moving TENGs, the contact area has a significant impact on their outputs. Because the film thickness plays a large role in the induced charges, the induced charges are dominant since the electrodes touch instantly in normal-directional moving TENGs. In addition, the triboelectric charge is formed in the triboelectric layer through the friction of electrode materials, and then the dielectric layer material has triboelectric charges on the surface. However, the induced charge is related to the dielectric layer thickness and the electrode spacing of the constant capacitance formed by TENG. The induced charge comes from the induction of the charge held by the triboelectric layer. Consequently, the triboelectric charges are key to the performance of TENGs and are significantly more influential than the induced charges.

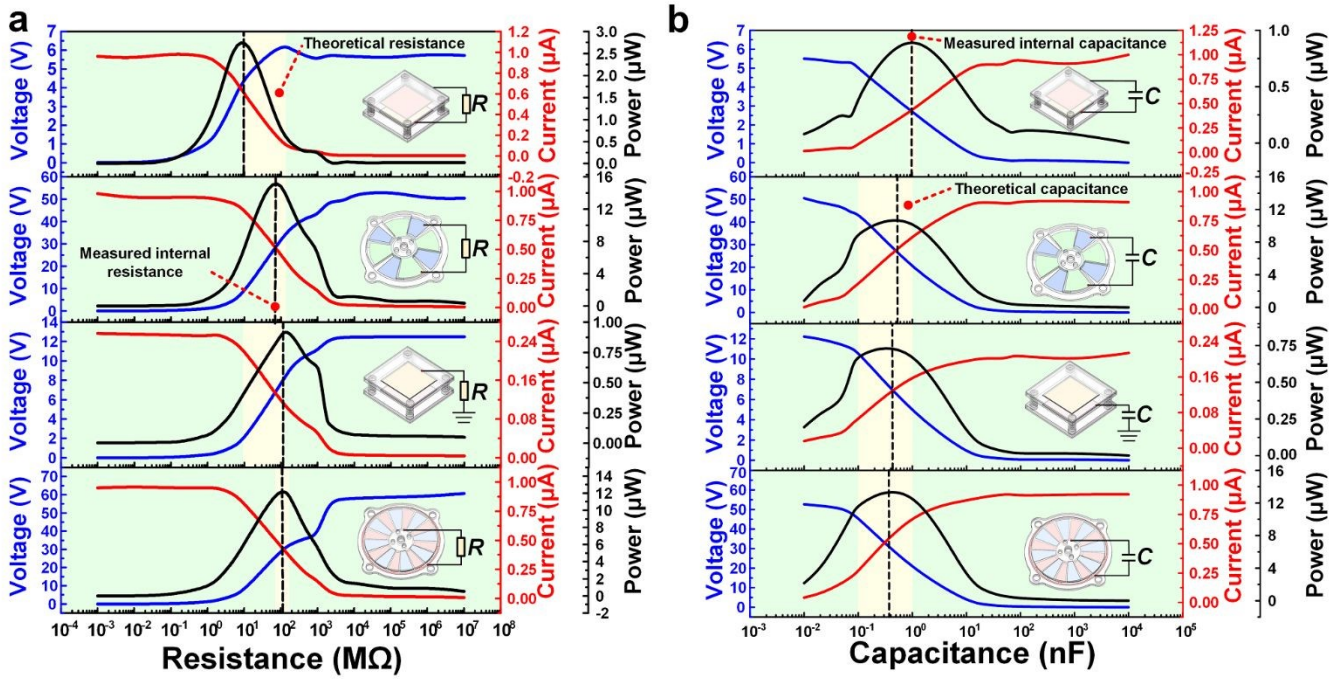

Fig. 6. Theoretical calculation and performance test of matching resistance (**a**) and matching capacitance (**b**) of different mode prototypes.

Measurement and verification of the normalization method.

Prototypes are fabricated based on the four modes (Fig. S12) (ESI†), the specific parameters of which are shown in Table S3 (ESI†). In particular, matching resistance and capacitance are determined by measuring the load voltage, current, and peak power. As shown in Fig 6, the matching resistance and capacitance are about MΩ and nF levels, respectively. Compared to S-E and F-S modes, C-S mode TENGs have the lowest resistance. However, the matching capacitance is larger for C-S mode and smaller for F-S mode. According to the equation of resistance and capacitance, the internal resistance or capacitance of TENGs can be calculated theoretically.

View Article Online
DOI: 10.1039/D2EE01553F

The calculation method and value of theoretical resistance and capacitance are presented in Supplementary Note 2 and Table S4 (ESI†). By comparing experimental and theoretical data, this method is proven to be reasonable in predicting the optimal matching resistance and capacitance of TENGs to determine the output performance.

Conclusions

In summary, a quantitative standard based on internal equivalent circuit is proposed to assess the effects of the mechanical structures and external excitations on the outputs of the TENGs in various modes. This paper clarifies the relationship between equivalent circuit and TENGs, and then investigates the influence of mechanical structures (*e.g.* contact area, film thickness) and external excitations (*e.g.* applied force, displacement distance, triggering frequency) on output power and matching reactance by the normalization method. Experimental results show that the importance of influencing factors is: contact area > film thickness > applied force > displacement distance. That is, the mechanical structures have a greater influence on performance than the external excitations. The influence of triggering frequency on the normal-directional moving TENG is greater than that of the tangential-directional moving TENG. Moreover, the prototypes are fabricated to verify the rationality and feasibility of normalization. This work will provide a reference for TENG design and its practical application.

Experimental

Fabrication of prototypes.

The prototypes use acrylic as substrates. The dielectric layer and electrodes are made of polytetrafluoroethylene (PTFE) of thickness 80 μm and coppers of thickness 100 μm, respectively. Circular electrodes with a diameter of 30 to 70 mm are used in TENGs of normal moving mode. And TENGs of tangential moving mode adopts rectangular electrodes with a contact area of 50 mm× 50 mm. The parameters of the validated prototype are shown in Table S3 (ESI†).

Measuring device.

The output performance of TENG was measured in a constant temperature and humidity box (ATH Scientific, ATH-GLB-400SD, China) at 25 ℃ and 45% RH, respectively. Linear test system (dream, R-LP3, China) and two-phase hybrid servo motor (Vimidi, DE60HB102-1000, China) are employed to provide the external excitation. Moreover, the frequency conversion motion is frequency modulated by a self-made controller. The F-S mode TENG with flexible blades is used for triggering frequency conversion test (Fig. S13) (ESI†), and triggering frequency is controlled by a Micro Control Unit (STM32). The programmable electrometer (Keithley, 6514, USA) is employed to measure the output performance. The signal is collected by data acquisition system (DA-ARM1651) and displayed by LabVIEW software.

Data processing

The change of various factors will lead to the change of internal resistance and capacitance, which will affect the matching reactance of TENGs. Based on the theoretical equation, the load resistance or capacitance is transformed to equal proportion to the normalize matching reactance of TENGs (Figs 2, S4, 3, S7, 4 and S10) (ESI†). Moreover, according to the Eqs. (S14, S15) (ESI†), the load voltage and current are compared with the open-circuit voltage and short-circuit current respectively, so as to normalize the load performance (Figs. S2, S3, S5, S6, S8 and S9) (ESI†). In addition, the peak-to-peak power of all the collected factors is compared to the maximum peak-to-peak power of all the factors to achieve normalization of the output power (Figs.5 and S12) (ESI†).

Author contributions

Z. L. W. and T. C. supervised and guided the project; T. C., X. Y., D. Z. J. W. and Q. G. conceived the idea, discussed the data and prepared the manuscript; D. Z., J. W. and Z. W. fabricated the devices, designed the measurement and performed the experiments; X. Y., D. Z., J.W and Z. W proposed the model and analysed the data. All the authors helped revise the manuscript.

Conflicts of interest

The authors declare no competing financial interest.

Acknowledgements

The authors are grateful for the support received from the National Key R & D Project from Minister of Science and Technology (Nos. 2021YFA1201601 &

2021YFA1201604) and the Beijing Natural Science Foundation (No. 3222023).

References

1. F. R. Fan, Z. Q. Tian and Z. L. Wang, *Nano energy*, 2012, **1**, 328-334.
2. Z. L. Wang, *Rep. Prog. Phys.*, 2021, **84**, 096502.
3. H. Wang, J. Cheng, Z. Wang, L. Ji and Z. L. Wang, *Sci. Bull.*, 2021, **66**, 490-511.
4. Z. L. Wang, *Adv. Energy Mater.*, 2020, **10**, 2000137.
5. Z. L. Wang, *ACS Nano*, 2013, **7**, 9533-9557.
6. Gao, F. et al. F. Gao, Z. Zhang, Q. Liao, G. Zhang, Z. Kang, X. Zhao, X. Xun, Z. Zhao, L. Xu, L. Xue and Y. Zhang, *Adv. Energy Mater.*, 2019, **9**, 1901881.
7. Z. Wu, T. Cheng, and Z. L. Wang, *SENSORS-BASEL*, 2020, **20**, 2925.
8. R. D. I. G. Dharmasena, K. D. G. I. Jayawardena, C. A. Mills, J. H. B. Deane, J. V. Anguita, R. A. Dorey and S. R. P. Silva, *Energy Environ. Sci.*, 2017, **10**, 1801-1811.
9. J. Chen, Y. Huang, N. Zhang, H. Zou, R. Liu, C. Tao, X. Fan, Z. L. Wang, *Nat. Energy*, 2016, **1**, 1-8.
10. D. Zhao, X. Yu, Z. Wang, J. Wang, X. Li, Z. L. Wang and T. Cheng, *Nano Energy*, 2021, **89**, 106335.
11. H. Zou, Y. Zhang, L. Guo, P. Wang, X. He, G. Dai, H. Zheng, C. Chen, A. C. Wang, C. Xu and Z. L. Wang, *Nat. Commun.*, 2019, **10**, 1427.
12. X. Xie, X. Chen, C. Zhao, Y. Liu, X. Sun, C. Zhao and Z. Wen, *Nano Energy*, 2021, **79**, 105439.
13. M. Yin, X. Lu, G. Qiao, Y. Xu, Y. Wang, T. Cheng and Z. L. Wang, *Adv. Energy Mater.*, 2020, **10**, 2000627.
14. N. Cui, C. Dai, J. Liu, L. Gu, R. Ge, T. Du, Z. Wang and Y. Qin, *Energy Environ. Sci.*, 2020, **13**, 2069-2076.
15. R. Lei, Y. Shi, Y. Ding, J. Nie, S. Li, F. Wang, H. Zhai, X. Chen and Z. L. Wang, *Energy Environ. Sci.* **13**, 2020, 2178-2190.
16. S. Niu, Y. Liu, S. Wang, L. Lin, Y. S. Zhou, Y. Hu and Z. L. Wang, *Adv Funct. Mater.*, 2014, **24**, 3332-3340.
17. J. Shao, T. Jiang, W. Tang, L. Xu, T. W. Kim, C. Wu, X. Chen, B. Chen, T. Xiao, Y. Bai and Z. L. Wang, *Nano Energy*, 2018, **48**, 292-300.
18. Y. Zi, H. Guo, Z. Wen, M.-H. Yeh, C. Hu and Z. L. Wang, *ACS Nano*, 2016, **10**, 4797-4805.
19. Z. Wang, W. Liu, J. Hu, W. He, H. Yang, C. Ling, Y. Xi, X. Wang, A. Liu and C. Hu, *Nano Energy*, 2020, **69**, 104452.
20. L. Lin, S. Wang, Y. Xie, Q. Jing, S. Niu, Y. Hu and Z. L. Wang, *Nano Lett.*, 2013, **13**, 2916-2923.
21. X. Kang, C. Pan, Y. Chen and X. Pu, *RSC Advances*, 2020, **10**, 17752-17759.
22. J. Shao, W. Tang, T. Jiang, X. Chen, L. Xu, B. Chen, T. Zhou, C. R. Deng and Z. L. Wang, *Nanoscale*, 2017, **9**, 9668-9675.
23. W. Tang, T. Jiang, F. Fan, A. Yu, C. Zhang, X. Cao and Z. L. Wang, *Adv. Funct. Mater.*, 2015, **25**, 3718-3725.
24. Y. Liu, W. Liu, Z. Wang, W. He, Q. Tang, Y. Xi, X. Wang, H. Guo and C. Hu, *Nat. Commun.* 2020, **11**, 1599.
25. C. Ye, K. Dong, J. An, J. Yi, X. Peng, C. Ning and Z. L. Wang, *ACS Energy Lett.*, 2021, **6**, 1443-1452.
26. S. Niu, Y. Liu, X. Chen, S. Wang, Y. S. Zhou, L. Lin, Y. Xie and Z. L. Wang, *Nano Energy* 2015, **12**, 760-774.
27. M. L. Seol, J. W. Han, D. I. Moon and M. Meyyappan, *Nano Energy*, 2017, **32**, 408-413.
28. W. Yang, X. Wang, H. Li, J. Wu, Y. Hu, Z. Li and H. Liu, *Nano Energy*, 2019, **57**, 41-47.
29. Z. Zhao, L. Zhou, S. Li, D. Liu, Y. Li, Y. Gao, Y. Liu, Y. Dai, J. Wang and Z. L. Wang, *Nat. Commun.*, 2021, **12**, 4686.
30. N. Cui, L. Gu, Y. Lei, J. Liu, Y. Qin, X. Ma, Y. Hao and Z. L Wang, *ACS Nano*, 2016, **10**, 6131-6138.
31. N. Cui, J. Liu, Y. Lei, L.Gu, Q. Xu, S. Liu and Y. Qin. *ACS Appl. Energy Mater.*, **6**, 2018, 2891–2897.
32. R. D. I. G. Dharmasena, *Nano Energy*, 2020, **76**, 10504.
33. M. Willatzen and Z. L. Wang, *Nano Energy*, 2018, **52**, 517-523.
34. S. Zargari, A. Rezania, Z. D. Koozehkanani, H. Veladi, J. Sobhi, L. Rosendahl, *Nano Energy*, 2022, **92**, 106740.
35. F.-R. Fan, W. Tang, Y. Yao, J. Luo, C. Zhang and Z. L. Wang, *Nanotechnology*, 2014, **25**, 135402.
36. C. Zhang, W. Tang, C. Han, F. Fan and Z. L. Wang, *Adv. Mater.* 2014, **26**, 3580-3591.